NANO: Brief Reports and Reviews
Vol. 12, No. 11 (2017) 1750134 (9 pages)

DOI: 10.1142/S179329201750134X

World Scientific
www.worldscientific.com

Development of Optimal Nanocrystalline Absorption Layer for Thin Film Silicon Solar Cell Applications

C. Álvarez-Macías*, J. D. Escobar-Carrasquilla†, A. Dutt†, E. Mon-Pérez†, L. González† and G. Santana†,‡

*Instituto Tecnológico de la Laguna, División de Estudios de Posgrado e Investigación Boulevard Revolución y Av. Instituto Tecnológico de la Laguna s/n, Col. Centro, Apartado Postal 681, C.P. 27000 Torreón, Coahuila, México

†Instituto de investigaciones en materiales, Universidad nacional autónoma de México A.P. 70-360, Coyoacán C.P. 04510, México, D.F.

‡gsantana@iim.unam.mx

Received 27 April 2017
Accepted 13 September 2017
Published 17 October 2017

To obtain an optimum absorption layer based on hydrogenated polymorphous and nanocrystalline silicon thin films in a plasma-enhanced chemical vapor deposition, radio frequency (RF) power was varied from 25 W to 100 W using a mixture of dichlorosilane and hydrogen. By Raman spectroscopy, the crystalline fraction was found to be varied from 7% to 69%, and RF power value of 75 W was found to be suitable with an appropriate mixture of amorphous and crystalline phases, respectively. Thickness measurements performed by profilometry were cross-checked with the value obtained from the cross-sectional scanning electron microscopy micrographs. Micrographs obtained using high-resolution transmission electron microscopy confirmed the presence of silicon nanocrystals in the range of 2–5 nm with a strong probability of confinement effect. B and gap value of 1.55 eV at 75 W upheld the suitability of this particular RF power for active absorption layer, which has also shown maximum photosensitivity.

Keywords: pm-Si: H; chemical vapour deposition; silicon thin film; band gap; absorption layer; photosensitivity.

1. Introduction

Investigation in the field of solar cells is getting much attention in the present world to satisfy the energy needs. Fabrication of efficient solar cells with the surplus advantage of cost effectiveness is a defining problem in modern society. When comparing the modern day solar cells (thin film technology) with their counterpart (bulk material), it has been found that the reduction in thickness of the active layer, in that case, comes at the cost of a decline in the efficiency.[1–4] This fact is common for silicon thin film solar cells, which is one of the most commonly used materials as an active layer (absorption region). Apart from that one of the biggest problems

‡Corresponding author.

with the silicon solar cell is the limitation that they cannot absorb in the near infrared region of solar spectra.[2] Additionally, in the case of solar cells, one of the leading causes of the loss is due to the absorbance of photo-excited carriers with energy higher than the band gap of the absorbing material (thermalization process).[5,6] Improving the absorption efficiency is thus a crucial part of designing the efficient modern thin-film silicon solar cells.[7–12] Hence, one of the anticipated factors is to design efficient solar cells with additionally controlling the solar spectrum absorption more efficiently at different wavelengths.

Already some research works exist on the modification or the improvement of the silicon absorption layers for the enhancement in the efficiency of a-Si:H solar cell.[13–18] Among the various factors, one of them is to manage the limitation of energy loss due to the inefficient absorption, which is called as band gap engineering.[19,20] As of now, after significant development in the investigation of this specific field, tandem solar cells, which is the third generation of solar cells, have proved their potential advancement in the area.[21,22] However, due to the limitation of Staebler–Wronski effect, a resultant reduction in the efficiency by 20–30% in the case of a-Si:H solar cells provoked the investigation of other materials.[23] Moreover, tandem cells also suffer from some of the drawbacks such as the use of numerous precursor gases, complex design (overcoming the economic process), overheating of the different cells connected either in series or in parallel connection due to mismatch and limitations of short-circuit current.[24]

Consequently, in the last few years, research on the fabrication of polymorphous (pm-Si:H) and nanocrystalline silicon (nc-Si:H) has been done.[25,26] These materials consist of different silicon crystalline phases (nanocrystals and microcrystals) embedded in an amorphous silicon matrix. Key benefits of these materials are greater doping efficiency, better electrical conductivity and lower defect densities.[27,28] Besides, the two-phased morphological configuration of these materials, which consists of Si crystallites embedded in an amorphous matrix, makes these materials as likely candidates for more stable high-efficiency solar cells.[29] Moreover, depending on the deposition conditions, one could vary the crystallization fraction as well as size of the nanoparticles (observed in the present work) to finally attain the stable optoelectronic properties combining the benefits of simple, economic fabrication technique. Besides, pm-Si:H thin films have a surplus advantage of being more stable in the environment due to the absence of SiH_m absorption bands.[26]

In our past reports, we have shown the perspective of the dichlorosilane (SiH_2Cl_2) as silicon precursor compared with most frequently used precursor silane (SiH_4).[26,29,30] Advantages of the thin film obtained by using this unique precursor are being discussed in our earlier published work.[30]

In the present work, we have carried out intensive research on the development of silicon thin films with control over the transition from polymorphous to nanocrystalline phases to establish an appropriate absorption layer adjoining the advantages of dichlorosilane as a precursor in plasma-enhanced chemical vapor deposition (PECVD). Thin films deposited using this precursor allow fabricating the material with the property of band gap tuning, which is a surplus advantage for various optoelectronic applications. Additionally, in the current work, influence of different radio frequency (RF) powers on the crystalline fraction (X_c), thickness (in nm), band gap (in eV) and, finally, the $L_{\text{effective}}$ (effective length), which is the sum of diffusion length and drift length has been established. Overall, the relationship of the structural and optoelectrical properties of the thin films assisted to find a particular value of RF power, which could be used for the development of adequate absorption layer in the current generation of thin films silicon solar cells.

2. Experimental

pm-Si:H and nc-Si:H thin films in this work were fabricated by using the PECVD reactor operating at an *RF* of 13.56 MHz with parallel plates of 128 cm^2 in area and 1.5 cm apart. The system was maintained at 10^{-6} Torr before starting the deposition using a turbomolecular pump. Depositions were made on diverse substrate materials such as high resistivity (1 0 0) single crystalline silicon, fused silica (*quartz*) and glass, respectively, to carry out specific characterizations on each of them. The deposition conditions used in the present study are summarized in Table 1.

Table 1. Summary of the deposition conditions carried out in this work.

SiH_2Cl_2, H_2 and Ar flow rates	7.5, 50 and 50 sccm, respectively
Substrate temperature (T_s)	250°C
Chamber pressure	500 mTorr
Deposition time	30 min
RF power (in watts)	25, 50, 75 and 100

Raman spectroscopy was used to evaluate the structural information about the thin film via equipment model T6400 with Horiba Jobin-Yvon triple monochromator in backscattering configuration equipped with an Ar 532.1 nm (green) laser source with 15 mW at laser head. All the measurements were performed at room temperature under the ambient conditions. Film thickness and growth rates were determined with a Sloan Dektak IIA profilometer and confirmed by scanning electron microscopy (SEM) Micrographs in a Carl Zeiss Auriga field emission microscope. Bright field images and selected area electron diffraction (SAED) were obtained using a high-resolution transmission electron microscope (HRTEM) (JEOL-ARM 200F) at 200 kV with a wavelength of 0.027 Å equipped with an AZTEC OXFORD equipment for the chemical composition measurement.

Optical properties were studied through the standard transmission from *UV*–Vis spectroscopy measurement via model Filmetrics. The measurement range selected for the transmission spectra was between 200 nm and 1100 nm, and the band gap was calculated using Tauc's model. The conductivity under dark and artificial illumination (dark conductivity σ_d and photoconductivity σ_{ph}, respectively) measurements were performed with coplanar *Ag* electrodes. $I-V$ curves were measured using a Keithley 617 programmable electrometer on planar geometry using a halogen lamp with an intensity of 100 mW/cm^2. The ratio $PS = (\sigma_{ph} - \sigma_d)/\sigma_d$, called photosensitivity, was extracted in order to determine the quality of the pm-Si:H and nc-Si:H thin films and assists to find the relation with $\mu\tau$ parameter (mobility lifetime product for electrons and holes). Photoluminescence (PL) spectra were obtained using a Kimmon Koha He–Cd laser with excitation wavelength of 325 nm and output power of 20 mW at room temperature.

3. Results and Discussion

3.1. *Structural and morphological analysis*

Raman spectroscopy has been performed to describe quantitatively the variations of the crystalline volume fraction (X_c) of the films. Figure 1 shows the Raman spectra of all samples deposited at 25, 50, 75 and 100 W, respectively. As it is well known that in the case of Raman, two bands, one associated with the silicon transverse optical mode at 520 cm^{-1}, which is ascribed to the microcrystalline phase and other at 480 cm^{-1}, attributed to the amorphous phase give much information about the current

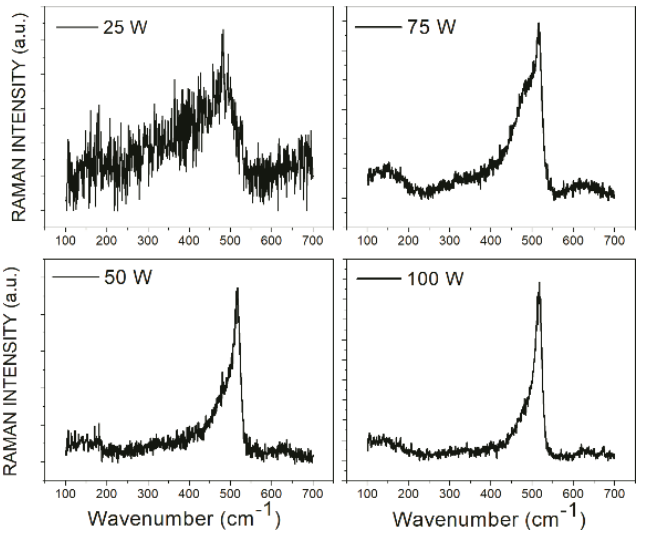

(a)

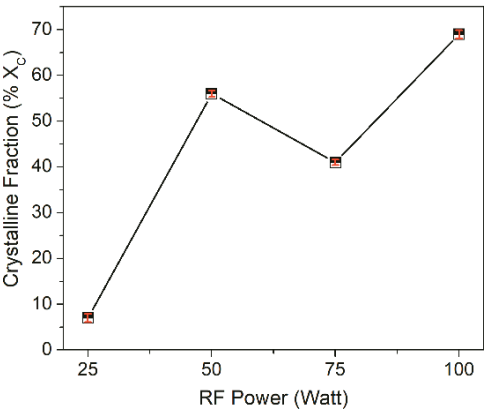

(b)

Fig. 1. (a) Raman spectra of the silicon thin films grown under the influence of different RF powers. (b) Calculation of the crystalline fraction (X_c) for various deposition RF powers.

phase of thin films.[31] Along with this, there could also be the presence of intermediate level from 500 cm^{-1} to 517 cm^{-1} related to the presence of small-sized nanoparticles and grain boundaries in the matrix. As mentioned in Sec. 1, pm-Si:H and nc-Si:H thin films consist of a mixture of an amorphous phase and a crystalline phase. Therefore, related characteristic peak could lie between the wavenumbers of 480 cm^{-1} and 520 cm^{-1}.

Obtained spectra of the thin films were analyzed by deconvoluting into three different peaks, two Lorentzian peaks corresponding to the microcrystalline (520 cm^{-1}), nanocrystalline (500–519 cm^{-1}) phase and another Gaussian peak for the amorphous phase (480 cm^{-1}). The areas of each peak were used to calculate the crystalline fraction (X_c). More details about the calculations could be viewed in our previous published work.[29]

From Fig. 1, it could be observed that as the RF power is increased from 25 W to 50 W, peak position shifted from 480 cm^{-1} to 517 cm^{-1}, which remark the transition in phase of the deposited material. The same could be crosschecked from Fig. 1(b) in which X_c increased from 7% to nearly 56%. Again, after increasing from 50 W to 75 W, a mixed phase (amorphous peak at 480 cm^{-1} and nanocrystalline peak at 514 cm^{-1}) could be observed from Fig. 1(a). Figure 1(b) shows the change in crystalline fraction from 56% to 41%, which validates the reduction in the crystalline phase. Finally, sample deposited at 100 W shows a strong narrow peak at 516 cm^{-1} and a crystalline fraction of 69%. In general, as a function of RF power, we can modify crystalline fraction from polymorphous silicon (25 W) to nanocrystalline phase (100 W).

Figure 2(a) shows, in general, variation in thickness of the different deposited samples. It can be inferred that the thickness increased from 100 nm to 400 nm by changing the RF power from 25 W to 100 W. For confirmation, Fig. 2(b) shows the cross-section of the sample deposited at 25 W and Fig. 2(c) of the sample deposited at 75 W. As can be seen from Fig. 2(a), thickness measured by profilometry for these specific samples is near around 105 nm and 150 nm, respectively, and from the cross-section SEM micrograph value obtained is around 111 nm and 141 nm, which shows real validation for the thickness measurements. Further detailed structural information of the nanoparticles was studied by HRTEM images. Figure 3(a) demonstrates the HRTEM image of the sample deposited at 25 W,

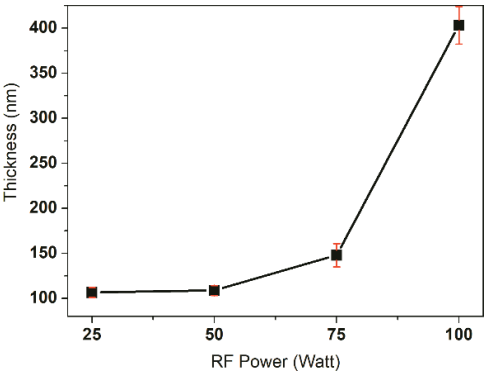

(a)

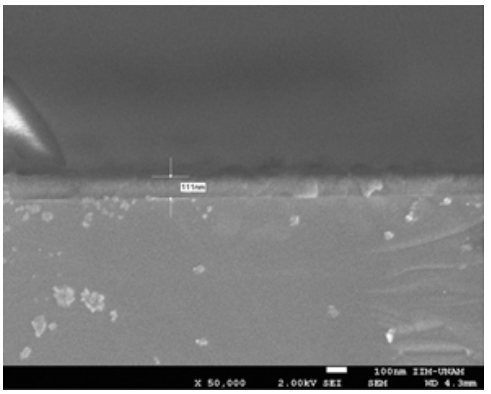

(b)

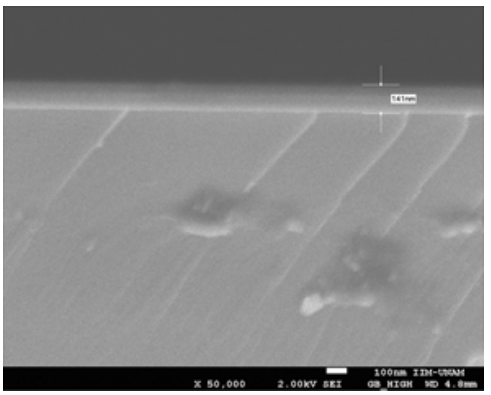

(c)

Fig. 2. (a) Thickness variation of silicon thin films deposited at different RF powers measured by using profilometry measurement; (b) and (c) cross-sectional SEM micrographs of the sample deposited at 25 W and 75 W, respectively.

and it can be observed that the thin film is composed of a random distribution of nanoparticles embedded in an amorphous matrix. The average size distribution of these nanoparticles estimated from HRTEM image is found to be around 2–5 nm,

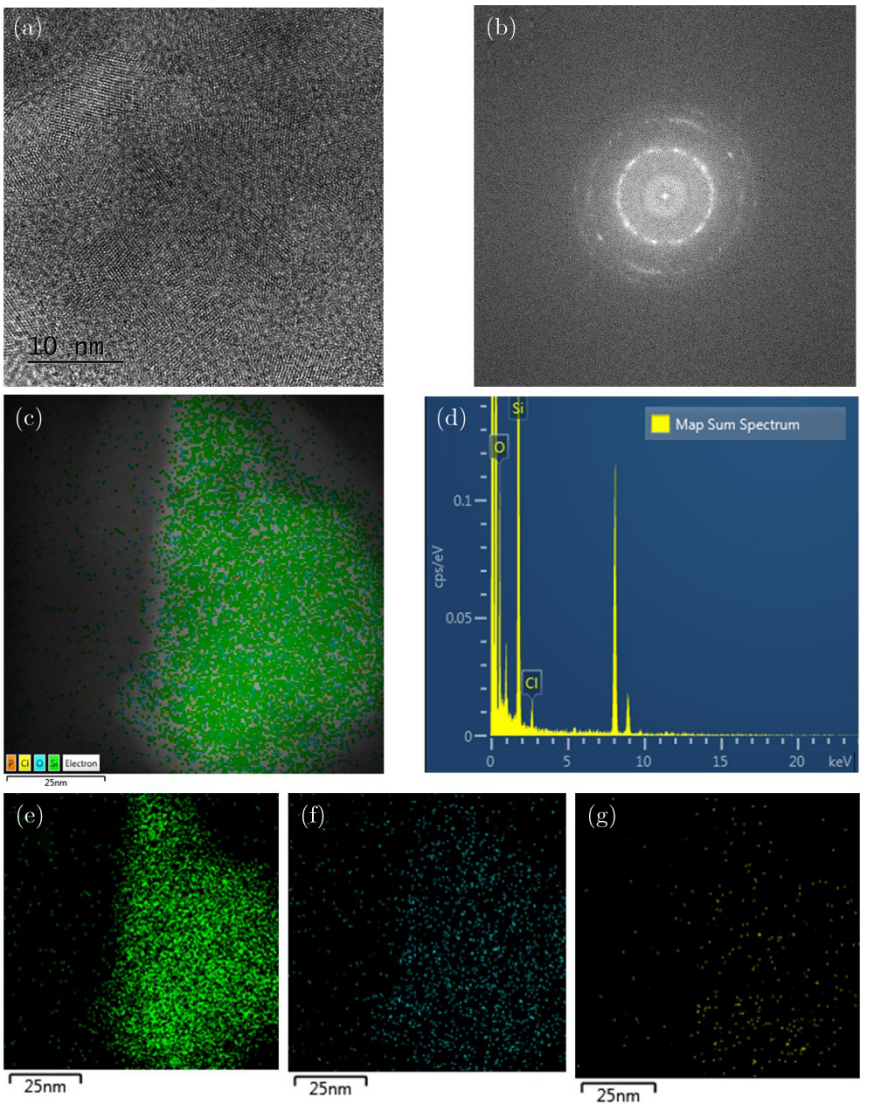

Fig. 3. (a) TEM image, (b) SAED pattern, (c) and (d) EDS spectra of silicon nanocrystalline embedded in an amorphous matrix. (e–g) STEM-EDS mapping profile of Si, O and Cl, respectively, in the crystalline region.

which is in concordance with the size estimation made using the spectral nanocrystalline peak shift (503–517 $cm^{-}1$) in the Raman spectra (Fig. 1). The presence of this size distribution of silicon nanoparticles could be related to quantum confinement effect (QCE). According to quantum confinement theory, the optical band gap E_{gop} depends on the size of the nc-Si as $E_{\text{gop}} \approx E_g + \hbar^2\pi^2/2\mu DR^2$, where E_g is the bulk material gap and μ is the reduced mass of electron–hole pair.[32]

Figure 3(b) shows the SAED pattern for one of the selected portions of the crystalline region illustrated in Fig. 3(a). SAED pattern remarks the high polycrystalline nature of the thin film deposited. EDS (energy-dispersive X-ray spectroscopy) patterns recorded from the sample deposited at 25 W is shown in Figs. 3(c) and 3(d), where it is shown the presence of Si, O and Cl elements. Moreover, scanning transmission electron microscope-energy-dispersive X-ray spectroscopy (STEM-EDS) mapping was also recorded to determine the homogeneous distribution of Si, O and Cl elements in the nanoparticles [Figs. 3(e)–3(g)]. Presence of Cl in the thin film is consistent with the use of dichlorosilane as a silicon precursor and shows the formation of as-deposited silicon nanoparticles [Fig. 3(a)] due to the chlorine chemistry in the thin films.[30]

3.2. *Optoelectronic characterizations*

Figure 4 demonstrates the effective absorption coefficient of the thin films with respect to different RF powers. The optical density data, in general, depend on numerous factors such as the content of silicon in different phases, hydrogen and microvoids in the films. In the present work, optical band gap values have been obtained from the transmission measurements in the range 200–1100 nm of the films grown on the quartz substrates. Inset in Fig. 4 shows the band gap association of silicon thin films with the variation in RF power. It can be observed that for this particular series of experiments, band gap variation from 1.45 eV to 2.0 eV is achieved, which confirms the possibility of band gap tuning by using dichlorosilane as precursor gases in as-grown samples. Decrease in the band gap value from 2.0 eV (25 W) to 1.45 eV (50 W), 1.55 eV (75 W) and lastly 1.75 eV (100 W) could be correlated to the variation in the crystalline fraction [Fig. 1(b)] and the change in the average size of silicon nanocrystals [shift in the Raman peak, Fig. 1(a)]. This kind of tendency observed here also remarks the role of quantum confinement in nanocrystals. Furthermore, it is important to mention here that neither the optical band gap (E_g) nor the nanocrystalline fraction percent (X_C) varies monotonically with the variation of RF power, and same kind of result has been demonstrated earlier in one of our previously published reports.[33]

The above-mentioned experiments have been performed repeatedly to confirm the role of RF power on the crystalline fraction, size of nanoparticles and hence on the band gap of the as-deposited thin film for their usage in practical implementation.

Figure 5 demonstrates the behavior of photosensitivity of the samples with variation in the RF power. This parameter is further correlated with the behavior of the $\mu\tau$ factor (inversely proportional to the concentration of dangling bonds in the thin film). It can be observed here that increasing the RF power from 25 W until 75 W caused a sudden hike in the photosensitivity and therefore in the $\mu\tau$ factor and as a consequence it could cause change in the effective length (diffusion and drift) of the final structure. It is worth noting that here likewise maximum photosensitivity can be observed for the sample deposited at 75 W. For this particular sample, the photosensitivity is almost 1.6×10^4, which is nearly one order more than compared with the other samples.

Generally, it is a well-known fact that during photoconductivity (sensitivity) measurements, there could be generation by absorption of extra electron and hole pairs. In that case, it is quite probable that the excessive lifetime of the electron and hole carriers could increase as well, which subsequently could increase the $\mu\tau$ factor. Moreover, as the absorption layer proposed in the present work will be used for the type p-i-n (n-i-p) structures, the situation could be more complex for the effective length in this case. The deciding factor could be drift length rather than diffusion length. In the case of type p-i-n (n-i-p) structure apart from the concentration gradient other import factor which could greatly influence the motion of electrons and holes is the applied electric field and in that case drift length is the parameter which comes into picture. The same is clear from the relation which states $L_{\text{Drift}} = \mu\tau.E$.

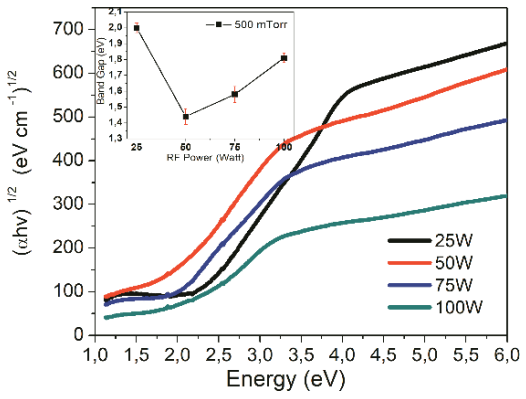

Fig. 4. UV–Vis spectra of silicon thin films grown under the influence of various RF powers.

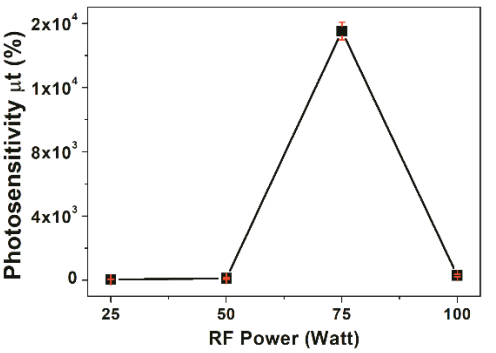

Fig. 5. The relation of photosensitivity of the material with the RF power with a maximum value attained for the sample deposited at 75 W.

Furthermore, this equation states the relationship of the $\mu\tau$ factor with the drift length. That is, the reason in the present case once having the estimation of change in relative photosensitivity, we can correlate with the $\mu\tau$ factor and hence with the drift length of the final structure. Higher is the photosensitivity better will be the value of $\mu\tau$ factor and higher will be the drift length, which is the required condition for an efficient structure. That is the reason, sample deposited at 75 W shows a good potential for the future fabrication of complete structure with less dangling bonds and higher drift length of the carriers.

It is important to discuss that crystalline fraction could play a very important role in the conductivity and effective length modifications (drift length in the present case) of samples. In the previous studies using various models such as grain-boundary trapping (GBT) and heteroquantum dots (HQD), the influence of the type of matrix and size of quantum dots on the conductivity of the deposited thin film has been explained.[34–36] According to the GBT model, polycrystalline silicon generally consists of small crystallites interconnected by a few disordered atomic layers and in that case carrier trapping could occur at the grain boundary. Conduction in these types of thin films is due to the thermal activation process. In the HQD model, distinct features of the conduction mechanism in these kinds of thin films have been explained. In this model, main consideration was focussed on the quantum dots. It was stated that the conduction in this case could occur due to quantum tunneling through interface barriers. Two of the above-mentioned models could similarly be correlated with the conduction process in pm-Si:H and nc-Si:H thin films. There could be three distinct cases:

(1) In the case of less dense nanoparticles, 25 W (a smaller proportion of crystallites in the film) conduction could occur through thermal activation process. Density of states and levels of energy could also play a significant role in this case.
(2) In the case of highly compact or dense particles (100 W) as mentioned above, the conduction could increase significantly due to the tunneling process.
(3) In the case of intermediate samples, 50 W and 75 W (mixed proportion of amorphous and crystalline phases), conduction could occur through both ways and this could be the reason for better conductivity in the case of mixed phase samples. Hence, these complex features could play a vital role in the values of the effective length modifications and lifetime of the minority carriers and furthermore conductivity (photosensitivity) of the material.

This behavior is totally in concordance with the trend of the crystalline fraction observed in Fig. 1(b) because the transport properties of the material could be greatly influenced by the morphology (grain size, grain boundaries and region of crystallization).[37] Crystalline fractions [Fig. 1(b)], band gap value (Fig. 4) and photosensitivity (Fig. 5) indicate the improvement in the optoelectronic properties of these materials observed for the sample deposited at 75 W.

After carrying out various structural, morphological and optical characterizations, PL (photoluminescence) studies were conducted on the samples. PL is an imperative tool to make the diagnosis of the film quality of the sample. Indirectly with the PL emission bands and with the corresponding wavelength or intensity, one can find out the defect distribution in the thin film.

From Fig. 6 it can be observed the PL spectra for the sample deposited at 25 W and 100 W. As the measurements had been carried out using 325 nm laser (3.8 eV) in the visible region, only luminescence with the naked eye in the ambiance from two samples (25 W and 100 W) can be seen. This is in concordance with the band gap values observed in Fig. 4. As mentioned earlier for the samples 25 W and 100 W band gap values are 2.0 eV and 1.75 eV, which according to the quantum confinement model

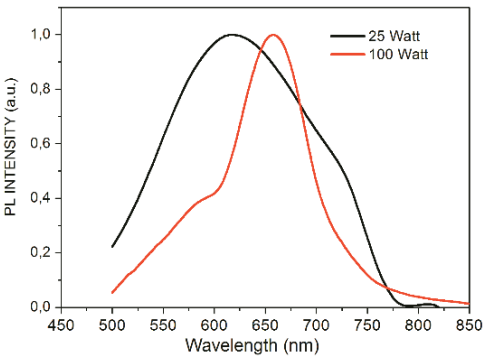

Fig. 6. Normalized PL spectra of the samples deposited at 25 W and 100 W measured by a He-CD laser at room temperature.

should give the emission in the visible region.[38] Furthermore, a red shift in the luminescence from almost 617 nm to 658 nm is greatly dependent on the increase in the average size of the nanoparticles, which is subsequently effected by the rise in RF power from 25 W to 100 W. In contrast, 1.45 eV (50 W) and 1.55 eV (75 W) values may give rise to PL but in the infrared region which is not possible to measure with the current detector equipped with our PL system.

It is well understood that in a thin film silicon solar cell, the intrinsic or absorber layer plays a very important role as it has the main function of absorbing the photons and hence generating electron–hole pairs. For higher efficiencies, this particular layer should exhibit a higher absorption coefficient to make sure the maximum generation of electron–hole pairs for a minimal thickness. Nevertheless, as discussed earlier, they suffer from major degradation problems with the course of time. For that reason, research on pm-Si:H and nc-Si:H is established because of high mobility values and reduced defect states when compared with conventional a-Si:H growth starting silanes precursors. Furthermore, in the case of pm-Si:H and nc-Si:H factor, $\mu\tau$ can be 100 higher than that of standard a-Si:H for samples in the as-deposited state.[39] This factor makes sure the high effective length (sum of diffusion ad drift) and conductivity or sensitivity values as is observed in the current work (especially for the sample deposited at 75 W). Moreover, as observed in the present work in the case of silicon thin films we could vary the band gap from 1.45 eV to 2.0 eV which could be reflected in the short circuit current (I_{sc}) and the open circuit voltage of the resultant device. Also, it has been reported that pm-Si:H and nc-Si:H have a tendency to show higher values of short circuit current due to the presence of specific material properties. Hence, better stability with improved voltage and current characteristics could result in a modern silicon solar cell with improved spectral response and efficiency limit values. Hence, the absorber layer with range of band gap values presented in the present work with lower defect densities (high photosensitivity and drift length) could be used in the design of future silicon thin film solar cells.

4. Conclusions

In summary, we have achieved variation in the optical band gap of pm-Si:H and nc-Si:H thin films grown at different RF powers using dichlorosilane as a precursor gas. Using Raman spectroscopy, phase nature of the thin films was determined. HRTEM images show the formation of nanoparticles in the range of 2–5 nm, whereas SAED pattern confirmed the well-defined polycrystalline phases. The real tendency was observed for the amorphous and crystalline phases, respectively, as we increased the RF power from 25 W to 100 W for this particular precursor in as-grown samples. Among all of the RF powers, 75 W was found to have an adequate mixture of amorphous, crystalline and polycrystalline nature. Maximum photosensitivity was also obtained for the same group of samples, and this fact shows proper optimization of optoelectronic properties. Experiments performed in the present work show real control over the deposition condition of pm-Si:H and nc-Si:H thin films of their use as in the absorber layer of the new generation of thin film silicon solar cells.

Acknowledgments

We acknowledge financial support from CONACyT Mexico for this work through doctoral and postdoctoral scholarships CVU 445952 and CVU 462696, respectively. We acknowledge partial financial support for this work from DGAPA-UNAM PAPIIT Projects IN108215, IN107017. We would express our sincere thanks to Josue E. Romero-Ibarra for SEM measurements and C. D. Ramos Vilchis and Cain González for technical assistance. We also thank M. Picquart from the physics department of UAM-I for Raman characterization, technical and information support.

References

1. M. A. Green, *IEEE Trans. Electron Devices ED.* **31**, 671 (1984).
2. A. Lin and J. Phillips, *Sol. Energy Mater. Sol. Cells* **92**, 1689 (2008).
3. P. Campbell and M. A. Green, *J. Appl. Phys.* **62**, 243 (1987).
4. R. Dewan and D. Knipp, *J. Appl. Phys.* **106**, 074901 (2009).
5. G. Conibeer, *Mater. Today* **10**, 42 (2007).
6. S. Chen, L. Zhu, M. Yoshita, T. Mochizuki, C. Kim, H. Akiyama, M. Imaizumi and Y. Kanemitsu, *Sci. Rep.* **7**, 1 (2015).
7. F. Meillaud, M. Boccard, G. Bugnon, M. Despeisse, S. Hanni, F.-J. Haug, J. Persoz, J.-W. Schuttauf,

M. Stuckelberger and C. Ballif, *Mater. Today* **18**, 378 (2015).
8. A. Shah (Ed.), *Thin-Film Silicon Solar Cells* (EPFL Press, CRC Press, 2010).
9. P. Cuony, D. T. L. Alexander, I. Perez-Wurfl, M. Despeisse, G. Bugnon, M. Boccard, T. Söderström, A. Hessler-Wyser, C. Hébert and C. Ballif, *Adv. Mater.* **24**, 1182 (2012).
10. C. Chen, R. Jia, H. Yue, H. Li, X. Liu, T. Ye, S. Kasai, H. Tamotsu, N. Wu, S. Wang, J. Chu and B. Xu, *Vac. Sci. Technol.* **29**, 021014 (2011).
11. M. Boccard, C. Battaglia, N. Blondiauxb, R. Pugin, M. Despeisse and C. Ballif, *Sol. Energy Mater. Sol. Cells*, **119**, 12 (2013).
12. B. Niesen, N. Blondiaux, M. Boccard, M. Stuckelberger, R. Pugin, E. Scolan, F. Meillaud, F.-J. Haug, A. Hessler-Wyser and C. Ballif, *Nano Lett.* **14**, 5085 (2014).
13. O. Vetterl, F. Finger, R. Carius, P. Hapke, L. Houben, O. Kluth, A. Lambertz, A. MuKck, B. Rech and H. Wagner, *Sol. Energy Mater. Sol. Cells* **62**, 97 (2000).
14. S. Yang, P. Liu, D. Ding, Q. Guo and Y. Chen, *Nano* **12**, 1750029 (2017).
15. R. Vanderhaghen, S. Kasouit, R. Brenot, V. Chu, J. P. Conde, F. Liu, A. de Martino and P. Roca i Cabarrocas, *J. Non-Cryst. Solids* **299**, 365 (2002).
16. T. Matsui, A. Matsuda and M. Kondo, *Sol. Energy Mater. Sol. Cells* **90**, 3199 (2006).
17. Y. Nakano, S. Goya, T. Watanabe, N. Yamashita and Y. Yonekura, *Thin Solid Films* **506**, 33 (2006).
18. M. Matsumoto, Y. Aya, A. Kuroda, H. Katayama, T. Kunii, K. Murata, M. Hishida, W. Shinohara, I. Yoshida, A. Kitahara, H. Yoneda, A. Terakawa, M. Iseki and M. Tanaka, *IEEE J. Photovolt.* **3**, 35 (2013).
19. X. Liua, W. Zi and S. (Frank) Liu, *Mater. Sci. Semicond. Process.* **39**, 192 (2015).
20. R. J. Zambrano, F. A. Rubinelli, W. M. Arnoldbik, J. K. Rath and R. E. I. Schropp, *Sol. Energy Mater. Sol. Cells* **81**, 73 (2004).
21. Y. Kurokawa, M. Yano, S. Miyajima and A. Yamada, *Jpn. J. Appl. Phys.* **56**, 04CS03-1 (2017).
22. J. P. Mailoa, C. D. Bailie, E. C. Johlin, E. T. Hoke, A. J. Akey, W. H. Nguyen, M. D. McGehee and T. Buonassisi, *Appl. Phys. Lett.* **106**, 121105-1 (2015).
23. K. Keya, T. Kojima, Y. Torigoe, S. Toko, D. Yamashita, H. Seo, N. Itagaki, K. Koga and M. Shiratani, *Jpn J. Appl. Phys.* **55**, 07LE03-1 (2016).
24. F. Meillaud, A. Shah, C. Droz, E. Vallat-Sauvain and C. Miazza, *Sol. Energy Mater. Sol. Cells* **90**, 2952 (2006).
25. K. Ha, E. Jang, S. Jang, J. K. Lee, M. S. Jang, H. Choi, J. S. Cho and M. Choi, *Nanotechnology* **27**, 055403 (2016).
26. A. Remolina, B. M. Monroy, M. F. García-Sánchez, A. Ponce, M. Bizarro, J. C. Alonso, A. Ortiz and G. Santana, *Nanotechnology* **20**, 1 (2009).
27. S. W. Kim and D. L. Choi, *Mater. Lett.* **64**, 975 (2010).
28. Z. X. Zhao, R. Q. Cui, F. Y. Meng, B. C. Zhao, H. C. Yu and Z. B. Zhou, *Mater. Lett.* **58**, 3963 (2004).
29. A. Remolina, L. Hamui, B. M. Monroy, M. F. García-Sánchez, A. Ponce, M. Picquart and G. Santana, *Phys. Status Sol. C* **8**, 850 (2011).
30. E. Mon-Pérez, J. Salazar, E. Ramos, J. S. Salazar, A. L. Suárez, A. Dutt and G. Santana, *Nanotechnology* **27**, 1 (2016).
31. K. Uchinokura, T. Sekine and E. Matsuura, *Solid State Commun.* **11**, 47 (1972).
32. J. D. Escobar-Carrasquilla, C. Álvarez-Macías, A. Dutt, E. Mon-Péreza, L. Huerta and G. Santana, *Thin Solid Films* **638**, 389 (2017).
33. B. M. Monroy, A. Remolina, M. F. Garcia-Sanchez, A. Ponce, M. Picquart and G. Santana, *J. Nanomater.* **1**, 1 (2011).
34. P. G. Lecomber, G. Willeke and W. E. Spear, *J. Non-Cryst. Solids* **59 & 60**, 795 (1983).
35. J. Y. W. Seto, *J. Appl. Phys.* **46**, 5247 (1975).
36. G. Y. Hu, R. F. O'Connell, Y. L. He and M. B. Yu, *J. Appl. Phys.* **78**(6), 3945 (1995).
37. K. Lips, P. Kanschat and W. Fuhs, *Sol. Energy Mater. Sol. Cells.* **78**, 513 (2003).
38. T.-Y. Kim, N.-M. Park and K.-H. Kim, *Appl. Phys. Lett.* **85**, 5355 (2004).
39. Y. Poissant, P. Chatterjee and P. Roca i Cabarrocas, *J. Appl. Phys.* **94**, 7305 (2003).